

***In situ* imaging and structure determination of bacterial toxin delivery systems using electron cryotomography**

Debnath Ghosal^{1,†}, Mohammed Kaplan^{1,†}, Yi-Wei Chang¹, Grant J. Jensen^{1,2*}

¹ *Division of Biology and Biological Engineering, California Institute of Technology,
Pasadena, CA, USA.*

² *Howard Hughes Medical Institute, Pasadena, CA, USA.*

**corresponding author: Jensen@caltech.edu*

† These authors contributed equally to this work

Abstract

Determining the three-dimensional structure of bio-macromolecules at high-resolution in their native cellular environment is a major challenge for structural biology. Towards this end, electron cryotomography (ECT) allows large bio-macromolecular assemblies to be imaged directly in their hydrated physiological milieu to ~4 nm resolution. Combining ECT with other techniques like fluorescent imaging, immunogold labeling and genetic manipulation has allowed the *in situ* investigation of complex biological processes at macromolecular resolution. Furthermore, the advent of cryogenic focused ion beam (FIB) milling has extended the domain of ECT to include regions even deep within thick eukaryotic cells. Anticipating two audiences (scientists who just want to understand the potential and general workflow involved, and scientists who are learning how to do the work themselves), here we present both a broad overview of this kind of work and a step-by-step example protocol for ECT and subtomogram averaging using the *Legionella pneumophila* Dot/Icm type IV secretion system (T4SS) as a case study. While the general workflow is presented in step-by-step detail, we refer to online tutorials, users manuals, and other training materials for the essential background understanding needed to perform each step.

Keywords: Bacterial secretion system, *Legionella* Dot/Icm T4SS, Electron cryotomography (ECT), Subtomogram averaging.

1. Introduction and overview

Most biomolecules cannot be fully understood unless they are studied in the context of their physiological milieu, i.e., the cell^{1,2}. However, due to the complex setting inside the cell it is usually a prerequisite to extract the biomolecule(s) of interest out of the cell in order to determine its (their) atomic structure *in vitro* using methods like X-ray crystallography, nuclear magnetic resonance (NMR) spectroscopy and single-particle electron microscopy³⁻⁵. Indeed, these approaches have produced many of the triumphs of modern science by revealing the structures of many biomolecular complexes, shaping our understanding of modern biology⁶⁻¹². The difficulty of purifying many challenging biomolecular complexes has, however, limited our understanding about those complexes. In the last two decades, the advent of electron cryotomography (ECT) has allowed large protein complexes to be visualized directly inside the cell. Moreover, docking high-resolution structures from crystallography, cryoEM and NMR into ECT reconstructions allows the building of atomic models of giant molecular machines, which can lead to important new mechanistic insights into their function¹³⁻¹⁶.

ECT allows the determination of the structure of large biomolecular complexes while they are still in the mosaic environment of the cell at ~ 4 nm resolution^{17,18}. By tilting the sample and taking a projection image at every one or few degrees and then back-projecting the images (Fig. 1A), a 3D reconstruction of the specimen, known as the tomogram, can be produced (Fig. 1B)¹⁹. As biological samples are very sensitive to electron radiation, and the radiation damages build up over the course of imaging, different schemes of tilting the sample have been developed to first record the crucial information (at low-tilt angles) than the less relevant (at high-tilt angles), including the bidirectional tilt-scheme and dose symmetric tilt-scheme²⁰ (Fig. 1C). To improve

the signal and resolution of the complex one can record many tomograms of many cells that have the complex of interest and then average the volumes where the complex is present. This averaging of the volumes of interest (known as subtomogram averaging) is like single-particle reconstruction but it uses 3D volumes instead of 2D projections¹⁷. By averaging tens to thousands of such volumes it is possible to increase the signal-to-noise ratio and obtain *in situ* structures at 1-4 nanometer resolution^{14,16,21-27}. Moreover, combining ECT with light microscopy (Correlative Light and Electron Microscopy: CLEM) allows one to target specific protein (-complex) of interest in the cell^{28,29}. In addition, recent developments in the instrument hardware like the introduction of phase plate³⁰, and direct electron detection cameras with improved quantum efficiency and fast readout for correcting sample motions during imaging have paved the way to study more challenging biological systems inside the cell³¹⁻³³.

As examples, ECT has played a major role to improve our understanding of bacterial secretion systems^{13,15,24,34-38}. Secretion systems are membrane-embedded complex molecular machines involved in the translocation of effector proteins, nucleoprotein complexes and small molecules across the cell envelope. Due to their size and complexity it is usually difficult to purify the complexes intact for *in vitro* studies. Hence, much of our current knowledge of secretion systems is derived from high-resolution structures of isolated parts of these complexes solved by X-ray crystallography, NMR or cryoEM single-particle reconstruction³⁹⁻⁴². Fortunately, ECT is able to visualize the secretion systems directly *in vivo*, generating insights into their structures^{13,15,24,34-38}.

With that general introduction, next, we take the *Legionella pneumophila* Dot/Icm T4SS as an example and provide a step-by-step workflow of how to perform ECT studies of bacterial secretion systems starting from cell growth and proceeding through sample preparation, plunge freezing, data acquisition and structure determination. Our purpose in providing this example protocol is to bridge the gap between the general review articles (which provide theory and context) and technical user's manuals for the different software packages we use (which provide numerous possible options). It is important to remember that both ECT and subtomogram averaging methods are rapidly evolving, but the principles and basic steps remain largely unaltered.

Note: For a good theoretical understanding of cryoEM, we recommend readers to watch the online course: "Getting Started in Cryo-EM" (<http://cryo-em-course.caltech.edu/>). For a visual tour of cryoEM sample preparation, grid preparation, microscope alignment and data collection, visit here https://www.youtube.com/playlist?list=PL8_xPU5epJdfd5fM2CjQItR-iRIIEIjk8

2. Materials

2.1 Bacterial culture

Legionella cells grow in Charcoal-yeast extract (CYE) and ACES-buffered yeast extract (AYE) media. Prepare all media using Milli-Q® water. To prepare plates, dissolve 10 g ACES and 10 g yeast extract in ~0.9 liter Milli-Q® water, adjust pH to 6.9 by adding KOH and finally fill the volume up to 1 liter. Add 2 g activated charcoal and 15 g agar, stir the solution and autoclave the media at 121 °C for 40 minutes. After autoclaving, cool down the media and this can be stored in cold-room for later use. Before starting the culture, add filter sterilized supplements (0.4 g L-Cysteine hydrochloride, 0.15 g Fe(NO₃)₃, and 0.2 g Thymidine). To prepare ACES-buffered yeast extract (AYE) media, everything remains same but no Agar is added.

2.2 Grids for ECT:

Generally, for tomography of *L. pneumophila* cells, we use copper R2/2 200 Quantifoil holey carbon grid (Quantifoil Micro Tools GmbH, Jena, Germany). However, for CLEM experiments copper R2/2 200 Quantifoil holey carbon Finder grids are particularly useful to facilitate navigation and correlation between the two imaging modalities. If cells are grown directly on grids, UV treated gold grids with Quantifoil holey carbon film are preferred over copper grids to avoid cytotoxicity. The gold grids are relatively fragile and should be handled with great care.

2.3 Gold fiducials:

Gold fiducials are usually added to the sample prior to freezing. A uniform distribution of fiducial markers is pivotal for good alignment of individual tilt images. To improve

homogenous distribution of colloidal gold fiducials and prevent their aggregation, we coat these particles with bovine serum albumin (BSA). Generally, we mix 1 ml of colloidal gold particles (Sigma-Aldrich, St. Louis, MO, USA) with 250 μ l of filtered 5% (w/v) BSA and vortex the mixture thoroughly. Subsequently, we centrifuge this mixture at 14,000 x g for 30 min, remove the supernatant and resuspend the pellet in 50 μ l of same supernatant. This resuspended, concentrated solution can be stored at 4° C for several weeks (see **Note 1**).

2.4 Grid glow discharge system:

Prior to use, grids are glow-discharged to clean them and impart hydrophilicity (for more details: https://www.youtube.com/playlist?list=PL8_xPU5epJdfd5fM2CjQItR-iRIIEIJK8). In our lab, we use an Emitech K100X glow-discharging device. For glow discharging, grids are placed on the “specimen platform” with carbon side up and the distance between the specimen platform and the electrode is set to 2 cm. After closing the system, grids are glow discharged with 15 mA negative discharge at 1×10^{-1} bar for 60 s. Depending on sample type, the current, discharge time and distance between the specimen platform and the electrode can be adjusted. We always use freshly glow-discharged grids for the subsequent freezing step (see **Note 2**).

2.5 Sample freezing instrument:

Various automated as well as manual plunge freezing units are commercially available. To vitrify *L. pneumophila* cells, we use a Vitrobot Mark IV device from Thermo Fisher Scientific (formerly FEI, Hillsboro, OR, USA)⁴⁴ (Fig. 2).

2.6 Choice of microscopes:

Data collection can be done using a 300 kV microscope such as the Polara F30 (FEI), Titan Krios (FEI), Titan Halo (FEI), and JEOL3200 (JEOL, Japan) or using 200 kV instrument, such as a Tecnai F20 (FEI) with cryo-holder (Gatan) or Talos Arctica (FEI). 200 kV instruments are mainly good for screening grids. Usage of energy filter is critical for improving the signal-to-noise ratio.

3. Methods

3.1 Growing bacterial cells:

Grow bacterial cells under conditions (temperature/inducer/shaking speed/genetic manipulations etc.) that facilitate the expression of the secretions system of interest (Fig. 2). Here, a couple of milliliters of *L. pneumophila* (Philadelphia-1, Lp02) cells are grown in ACES [N-(2-acetamido)-2-aminoethanesulfonic acid]-buffered charcoal yeast extract agar (CYE) or in ACES-buffered yeast extract broth (AYE) supplemented with ferric nitrate and cysteine hydrochloride and thymidine ³⁴ (see Materials section). Since *L. pneumophila* is known to express the Dot/Icm T4SS at late exponential stage/early stationary stage, cells are harvested then and prepared for ECT. A good practice is to monitor the expression level by western blot and localization of the secretion system using fluorescence microscopy ³⁴. In cases where the secretion system only assembles when cells are grown on solid medium (like that of *Agrobacterium tumefaciens* conjugation machinery ⁴³), ~100 µl of the appropriate media is added onto the plate, and then the plate is gently washed to obtain the cells for ECT studies (see **Note 3**).

3.2 Plunge freezing of bacterial cells:

We maintain the vitrification chamber at 22 °C and 100% humidity using ddH₂O and vitrify cells using the following parameters: wait time 0s (time between application of sample onto the grid and blotting), blot-time 3-8s (time the filter paper blots excess liquid off the grid), drain time (time between end of blotting and plunge freezing) and a blot force of 6 (vertical position of the grid; this determines ice-gradient). To blot excess liquid off the grid, we use Whatman filter papers (diameter: 47 mm, grade-1). A hole is punched at the middle of these Whatman filter papers to allow it to assemble into the Vitrobot setup. When sample concentration or ice-thickness is inconsistent or desired structures are sheared during blotting process, manual blotting or blotting from a single side can be alternatively used. Optimizing sample blotting is extremely important for cryoEM. While less blotting leads to thick ice and reduces electron penetration, excessive blotting can result in drying artifacts. We generally add gold fiducials to the cells at 1:4 (v/v) and apply 4 µl of this mixture on to the carbon side of the grid. This is then plunge frozen in liquid ethane/propane mixture cooled by liquid nitrogen ⁴⁵ (see **Note 4**). Once frozen, grids are maintained at liquid nitrogen temperature, and for long-term storage, we generally keep the frozen grids in special grid-boxes (Ted Pella Inc) stored in liquid nitrogen dewars (see **Note 5**).

3.3 Data acquisition using UCSF TOMOGRAPHY:

After aligning the microscope, one can start acquiring tilt series (for more details:

https://www.youtube.com/playlist?list=PL8_xPU5epJdfd5fM2CjQItR-iRIIEIjk8).

Several softwares have been developed for tilt-series acquisition ⁴⁶⁻⁴⁸. Here, we will describe the

process that we follow in our lab using UCSF TOMOGRAPHY⁴⁸. First, scan the grid at low magnification (100x) to check the ice thickness in different areas of the grid and locate areas with thin ice where potentially data can be collected. For complete data collection to high-tilt angles, it is preferable to avoid areas near the edges of the grid. Then save the positions with thin ice in addition to the position of a broken/empty hole on the carbon film that can be used to optimize the beam as will be discussed later (see below). If no broken/empty place can be found on the grid, one can use continuous electron exposure to ‘punch’ a hole on the carbon film.

UCSF TOMOGRAPHY software has five different modes, which are: Atlas, Search, Track, Focus and Collect (Fig. 2 and Table-1). Calibrations are required for each of these modes.

Calibrate the system:

- 1- After starting the program, go to the broken/empty hole and center the electron beam. Set the exposure rate on the detector to $\sim 30 \text{ e}^-/\text{pixel}/\text{second}$ for all the modes in the “Calibration” as a starting point. After adjusting the beam in each mode go to “configure” and press “From scope”.
- 2- Set the parameters in each one of the five modes as illustrated in Table 1.
- 3- From the area with thin-ice determined at low magnification (100x), select two squares next (or close) to each other. One is for collecting data and the other is to perform the calibration steps. At the beginning of the calibration, we recommend adjusting the eucentricity of the area and then proceed with other calibrations. To ensure a smooth Calibration process select an area of the grid that is intact, flat and without major cracks and that is close to the area of data collection area. At the beginning of the calibration process, a distinct feature (dirt/ice crystal) should be selected and then following calibrations are required to be performed.
- 4- In the “Calibration”, perform the following:

- “Stage shift” for the “Atlas” and “Search” modes.
- “Image shift” for all the five modes.
- “Focus” for the “Track” and “Focus” modes.
- “Eucentric” for the “Track” mode.
- “Optical axis” for the “Focus” mode.
- “Align modes” should be done for the “Search” and “Collect” modes.

Record an Atlas and choose targets:

After the Calibration process is done, an atlas map has to be built in the “Montage”. First go to the area where data will be collected then determine area of interest for data collection (usually it is between 1-4 squares). Then provide values for atlas area, start the process by clicking the “Build” button (Fig. 2).

When the atlas map is done, upload it and examine the different parts of the map. Double clicking a tile in the Atlas map will enlarge that area and that will allow one to select potential targets by double clicking on them. A red circle will appear on the clicked area. Note that the first area double-clicked in each tile will be used to tune defocus, eucentricity and zero loss peak alignment of the energy filter (Fig. 1A). Pressing the right click on a selected area will deselect it. When all the targets have been selected this atlas map can be uploaded in the “Target” panel and medium magnification images of potential targets can be collected by clicking “Acquire Targets” button. Here, an image of each selected target will be taken in the “Search” mode (which has a magnification of 9300x in this example, see Table 1). When the process of collecting targets is finished a new file will be created with the same name of the Atlas map file but with “tgt” appended to the name of the file. The “tgt”-appended file can then be loaded in the “Target Review” panel where the collected images (at 9300x magnification) will be

displayed. Double-clicking on a target will select that for subsequent data collection in the “Collect” mode (which will be performed at 27,500x magnification in this example, See Table 1). The total number of targets selected for data collection will be displayed on the screen in the field “Total” in the “Target Review” panel. Before starting data collection, the electron counts in this region need to be set to (8-10 e/pixel/second). Once the exposure is set to 8-10 e/pix/s over the target area then go to the broken/empty hole and check the exposure again. The number of the electrons passing through the hole represent the total dose rate on the target and it will be used to calculate the data collection exposure time as explained below.

Tilt series acquisition:

Go to the “Tomography” panel and define the minimum (Min) and maximum (Max) angles of the tilt series and the exposure time. To calculate the exposure time, the following equation can be used:

Exposure time (s) = [Total Dose (e/A²) x (Pixel size (A))²] / [(Dose measured e/pix/s)x(Number of images in the tilt series)], where

The Total dose is between 100-200 e/A² depending on the sample.

Pixel size depends on the magnification of the collection mode (See Table 1).

Dose measured is the number of electrons (e/pix/s) passing through the hole.

Number of tilt images in the tilt series depends on the maximum and minimum tilt angles and the angular increment (e.g., for a tilt series from -60° to 60° with steps of 1° there will be 121 images)

3.4 Tilt series data processing/tomographic reconstruction

Tomographic reconstruction

Beam-induced specimen damage and movement during data collection result in blurred images. Therefore, especially for high-resolution projects, tilt images are often recorded in movie mode (dose fractionation mode). Subsequently, subframes are computationally aligned, averaged and saved. We often use the program MotionCor2 by Shawn Zheng and colleagues to correct for the beam induced movement ⁴⁹.

Initial setting up

From the motion corrected tilt-series, tomograms are reconstructed using the program IMOD ^{47,50,51}. IMOD homepage provides links to useful tutorial

(<http://bio3d.colorado.edu/imod/doc/tomoguide.html>) and videos

(<https://www.youtube.com/playlist?list=PLGggUwWmzvs9212cjWLb4hFOvdKJO1Y5O>) for users.

First, the motion corrected tilt-series are opened (“Build Tomogram”) using the IMOD program Etomo’s graphical user interface (GUI). Then, diameters of the gold fiducials and tilt-series axis type are specified as appropriate. Following this step, pixel size and image rotation are scanned from the tilt-series by clicking the option “Scan header”. At this point, it is advisable to examine the tilt-series by clicking “View raw image stack” to identify any bad frames that are to be excluded (“Exclude views”) during the reconstruction process. Then click “Create Computer Scripts”. Following this, there are several steps (Pre-processing → Coarse Alignment → Fiducial Model Gen. → Fine Alignment → Tomogram Positioning → Final Aligned Stack Complete → Tomogram Generation → Post-processing → Clean up) that need to be completed as listed in the Etomo GUI window. Each of the clickable tabs on the GUI provides information about the function if the cursor is hovered over it and turns gray after execution.

Pre-processing

This step helps in eliminating pixels with extremely low or high values that can generate artifacts. The program “Ccderaser” is used to remove all such extreme pixels. Use value 10 for “Peak criterion” and 8 for “Difference criterion” and then “Create Fixed Stack” followed by examination of the tilt series using “View Fixed Stack” and then click “Use Fixed Stack”. Once each of the steps is completed, proceed to the next section.

Coarse Alignment

In this step images are aligned based on cross-correlation. This helps in subsequent auto-tracking of fiducials for finer alignment of the tilt-series. First click “Calculate Cross-Correlation.” Then, use a “Coarse aligned stack binning” of 2 and click “Generate Coarse Aligned Stack”. Inspect this by clicking “View Aligned Stack in 3dmod” and fix any misalignment with “Midas”.

Fiducial Model Generation

There are three ways to select (typically 10-30) gold fiducials and track them through the tilt-series. These are “Make seed and track”, “Patch Tracking” and “Raptor”. We typically use “Make seed and track”. For this, select the “Make seed and track” radio button, provide the number of beads to track, activate “Refine center with Sobel filter” and provide a value 5. Then, click “Generate Seed Model”. Examine the seed model and then click “Track Seed Model” within “Track beads” subwindow. Fix any untracked or mis-tracked beads manually by opening “Fix Fiducial Model”.

Fine Alignment

In this step images are transformed so that they appear as projections of an object rotated around Y-axis. Click “Compute Alignment” and rectify any inappropriately placed fiducials by clicking “View/Edit Fiducial Model.”

Tomogram Positioning

For *L. pneumophila* cells, we use sample tomogram thickness 600 for cellular tomography. Click “Create Whole Tomogram” with a binning of 3 and then click “Create Boundary Model”. At this stage, rotate the tomogram 90°, indicate boundaries of the cell by drawing two horizontal lines, save the model and click “Create Final Alignment” that will run the program “tiltalign” with the final parameters.

Final Aligned Stack

The only thing we do here is “Create Full Aligned Stack”. When desired, this step also offers “Contrast Transfer Function (CTF) correction”, “Erase Gold” and “2D Filter” options.

Tomogram Generation

In this step a tomogram is built from a fully aligned image stack. A tomogram can be generated by either of the two options: 1) Weighted Back Projection, 2) Simultaneous Iterative Reconstruction Technique (SIRT) ⁵². SIRT reconstructions can be also generated separately by the program Tomo3D. View the generated tomogram by “View Tomogram in 3dmod” and if satisfied proceed to next step. The reconstructed tomogram (.rec file) can be opened anytime by the command *3dmod “file-name”*.

Post-processing

In this step, “Trim Volume” can be used to crop out a part of the tomogram with the object of interest or simply re-orient the tomogram. Note that reorientation of the tomogram can affect the handedness of objects within the tomogram.

Clean up

In this step intermediate files are deleted to free disk space. Note that there is an “XXX.edf” file. All the steps performed during the reconstruction process can be retrieved any time just by opening this file.

3.5 Subtomogram Averaging:

As mentioned earlier, subtomogram averaging can significantly enhance the signal-to-noise ratio and the resolution of selected subvolumes with repeated features (particles) within them. Different softwares can be used to achieve this goal like Dynamo, PEET, PyTom, Relion and several other programs^{22,50,53–56} (see **Note 6**). We generally use PEET to perform subtomogram averaging of bacterial secretions systems. A helpful user-manual for PEET can be found here: <https://bio3d.colorado.edu/PEET/PEETmanual.html>. There are several very useful tutorial videos for PEET, see here: https://www.youtube.com/watch?v=dUga1b_ON-c.

Picking particles

First open the tomogram with 3dmod then press the “Toggle between regular and high-resolution image” and “keep current image or model point centered” buttons which will show a red cross at the clicked area. These can be found on the upper left corner of the 3dmod slicer screen. After that, select the “Model” button in the small 3dmod window. Set the 3dmod slicer thickness to 10 and then go to “Edit” and select “Angles” to show the small angles window, which will display the angles and coordinates of the selected particles (Fig. 3). Subsequently, scan the different slices of the tomogram and rotate them accordingly to obtain the best view of your particle of interest and press the button “Save” on the upper left corner of the window to save these coordinates which will appear in the “Angles” window. Then use the middle click to

select the center of the red cross that is present on the selected particle and save the model as “*Name.mod*”. Repeat this process for all the particles in the tomogram and ultimately for all the tomograms.

Subtomogram averaging

When all the particles have been collected compute an initial motive list (MOTL) by running the command “stalkInit *Name.mod*” in the parent folder. Thereafter, create a new folder for the PEET run and then open PEET in the IMOD package and give a name to the run. Load all the tomograms and the corresponding models (*Name.mod* and the created MOTL files) in PEET. Enable missing wedge compensation by clicking the “Enable” box on the right-middle part of the window and supply the tilt angles (.tilt file). Fill the “Volume size” in voxels based on the particle size tool in 3dmod. Supply a reference for the run either by supplying the file for the best-looking particle or by defining the number of particles to be used for the reference (8, 16, 32, etc.) based on the total number of collected particles. No mask is usually used in the first run. Select the “Run” panel in the window and fill the iteration table as indicated by Table 2. The “Numbers of Particles to Average” fields (Start, Incr, End and Additional numbers) can be filled based on the total number of subvolumes to be averaged. As an example, in case of 33 particles fill 10 for each of the “start”, “Incr.”, 30 for the “End” and 33 for the “Additional numbers” which will result in subtomogram averages for 10, 20, 30 and 33 particles respectively. Click “Run” to start the subtomogram averaging.

3.6 Surface rendering, resolution estimation and deposition

When the first run is finished, the average can be visualized by clicking “Open averages in 3dmod” button at the bottom of the window. Based on the result of first run, subsequent runs

can be created using the “.prm” file of the first run and giving the first average as “Reference” for the second round. Appropriate masking of inner and outer membrane complexes can be used for subsequent focused alignment. The process can be repeated until there is no space for further improvement. For 3D surface rendered view of the average, use “Isosurface” (an isosurface is a surface where the intensity values are beyond certain threshold) view of the average.

UCSF Chimera program⁵⁷ is used to generate the final 3D surface view of the subtomogram average (<https://www.cgl.ucsf.edu/chimera/docs/UsersGuide/>). The resolution of the average can be estimated by Fourier shell correlation using PEET and local resolution can be calculated by ResMap⁵⁸ (<http://resmap.sourceforge.net/>). Once all these are done, the final step is to deposit the structure at the Electron Microscopy Data Bank (EMDB).

Figure legends:

Figure 1:

A) The principle of electron cryotomography. A field emission gun (FEG) produces the electrons that interact with the sample and are then detected by a camera to produce an image. The grid (sample) is rotated using an automated holder and an image of the sample is taken at each tilt angle (represented by grey lines). The images at different tilt angles are used to produce a 3D reconstruction known as the tomogram. The position of the energy filter is shown. **B)** A schematic representation of the principle of tomographic reconstruction. Images taken at different tilt angles are back-projected to reconstruct a 3D volume (the tomogram). The missing wedge is the area where no information can be obtained due to the infeasibility of tilting the sample to high angles. **C)** Different sample tilting schemes are present, these being (from left to right): the continuous tilt scheme, the bidirectional tilt scheme and the dose-symmetric tilt scheme. Darker areas in each tilt scheme correspond to where more information is present compared to the transparent areas. For further details, see (Hagen and Briggs, JSB, 2017).

Figure 2:

A work-flow to perform electron cryotomography and subsequent subtomogram averaging. *Legionella* cells are grown in culture (Culture), loaded onto EM grids, blotted, then plunge-frozen in liquid ethane/propane mixture (Vitrification). The grid can then be inserted into the EM and an Atlas can be produced for areas of good ice where data can potentially be collected (“Atlas” and “Tilt-series”). After reconstruction of the tomogram, particles of interest (T4SS in this example) can be picked from the reconstructed volume and an average can then be

calculated. The location of individual protein components can then be identified by imaging different mutant strains and generating a difference map with respect to the wild type structure. The local resolution of the structure can be calculated by ResMap and surface rendering can be done by UCSF-Chimera. The final structure should be then deposited in the EMDB.

Figure 3:

A) A schematic of a bacterial cell (*L. pneumophila* as an example) highlighting the location of the Dot/Icm T4SS particles at the cell pole. By inspecting slices of the tomogram and rotating them, standard orientation of each particle can be identified and saved. The selected subvolumes containing the particles can then be aligned and used to produce an average structure of the T4SS particle. **B)** A schematic of the parameters required to align subvolumes using PEET. A manually generated model for each particle (the red vector) is uploaded into PEET. Particles are aligned by allowing them to move within a distance defined by the user (search distance, see Table 2). The distance the particles are allowed to be moved can be determined by the user. Moreover, the particles are allowed to rotate around the three different axes X, Y and Z (represented by the dashed black, dashed green and dashed red lines respectively) as defined by the three angles Psi, Phi and Theta respectively. For further details, see Table 2.

Table 1:

Suggested parameters (Magnification, Defocus, Slit width, Exposure time, Binning, Spot size, Pixel size and Camera mode) are shown for each of the five different modes of UCSF TOMOGRAPHY (see **Note 7**).

Table 2:

A table showing the values typically used in PEET runs to generate subtomogram averages. See figure 3B for the definition of the different angles (Phi, Theta and Psi). The search distance is the translation allowed to align particles.

Acknowledgements:

We thank Dr. Songye Chen (Caltech). This work is supported by NIH grant R01482AI127401 to G.J.J.

4. Notes:

- 1) Some labs use protein-A conjugated 10 nm colloidal gold (Cell Microscopy Center, Utrecht University, The Netherlands) as fiducials.
- 2) In certain cases (e.g., eukaryotic cells), grids are treated with extracellular matrix proteins e.g. collagen, poly-L-lysine, or fibronectin, to improve the cell distribution and spreading.
- 3) For thicker bacterial/archaeal cells, specific growth media (e.g., starvation media/minimal media) or genetic manipulations can be used to grow thin cells. Sometimes, gentle antibiotic/lysozyme treatment can also help to image certain cellular features at higher-resolution.
- 4) Pure ethane can be used as a cryogen for vitrification. However, liquid ethane solidifies during sample freezing process. Thus, it needs to be warmed up periodically.
- 5) *L. pneumophila* is a BSL-2 pathogen hence extra care should be taken while growing and freezing these cells. Always wear proper lab coat, gloves, appropriate mask and eye protection. After freezing, clean the Vitrobot and the surrounding surface with 70% ethanol solution and all waste should be disposed in appropriately labeled Biohazard waste-container.
- 6) For more information about Relion, Dynamo, PyTom see following links:
Relion: https://www2.mrc-lmb.cam.ac.uk/relion/index.php?title=Download_%26_install
<https://www2.mrc-lmb.cam.ac.uk/relion/index.php?title=FAQs>
Dynamo: https://wiki.dynamo.biozentrum.unibas.ch/w/index.php/Starters_guide
PyTom: <http://pytom.org/doc/pytom/tutorial.html>

7) If phase plate is used for data collection, 0 or -0.5 defocus should be used. Phase plate modulates CTF and significantly enhances contrast.

References:

1. Sali, A., Glaeser, R., Earnest, T. & Baumeister, W. From words to literature in structural proteomics. *Nature* **422**, 216–225 (2003).
2. Robinson, C. V., Sali, A. & Baumeister, W. The molecular sociology of the cell. *Nature* **450**, 973–982 (2007).
3. Sali, A. & Kuriyan, J. Challenges at the frontiers of structural biology. *Trends Cell Biol.* **9**, M20-24 (1999).
4. Baumeister, W. & Steven, A. C. Macromolecular electron microscopy in the era of structural genomics. *Trends Biochem. Sci.* **25**, 624–631 (2000).
5. Curry, S. Structural Biology: A Century-long Journey into an Unseen World. *Interdiscip. Sci. Rev. ISR* **40**, 308–328 (2015).
6. Selmer, M. *et al.* Structure of the 70S ribosome complexed with mRNA and tRNA. *Science* **313**, 1935–1942 (2006).
7. Wimberly, B. T. *et al.* Structure of the 30S ribosomal subunit. *Nature* **407**, 327–339 (2000).
8. Groll, M. *et al.* Structure of 20S proteasome from yeast at 2.4 Å resolution. *Nature* **386**, 463–471 (1997).
9. Abrahams, J. P., Leslie, A. G., Lutter, R. & Walker, J. E. Structure at 2.8 Å resolution of F1-ATPase from bovine heart mitochondria. *Nature* **370**, 621–628 (1994).
10. Bui, K. H. *et al.* Integrated structural analysis of the human nuclear pore complex scaffold. *Cell* **155**, 1233–1243 (2013).
11. Carter, A. P., Cho, C., Jin, L. & Vale, R. D. Crystal structure of the dynein motor domain. *Science* **331**, 1159–1165 (2011).
12. Vinothkumar, K. R., Zhu, J. & Hirst, J. Architecture of mammalian respiratory complex I. *Nature* **515**, 80–84 (2014).

13. Basler, M., Pilhofer, M., Henderson, G. P., Jensen, G. J. & Mekalanos, J. J. Type VI secretion requires a dynamic contractile phage tail-like structure. *Nature* **483**, 182–186 (2012).
14. Chang, Y.-W. *et al.* Architecture of the type IVa pilus machine. *Science* **351**, aad2001 (2016).
15. Hu, B., Lara-Tejero, M., Kong, Q., Galán, J. E. & Liu, J. In Situ Molecular Architecture of the Salmonella Type III Secretion Machine. *Cell* **168**, 1065–1074.e10 (2017).
16. Beck, M., Lucić, V., Förster, F., Baumeister, W. & Medalia, O. Snapshots of nuclear pore complexes in action captured by cryo-electron tomography. *Nature* **449**, 611–615 (2007).
17. Briggs, J. A. G. Structural biology in situ--the potential of subtomogram averaging. *Curr. Opin. Struct. Biol.* **23**, 261–267 (2013).
18. Oikonomou, C. M. & Jensen, G. J. A new view into prokaryotic cell biology from electron cryotomography. *Nat. Rev. Microbiol.* **15**, 128 (2017).
19. Baumeister, W. Electron tomography: towards visualizing the molecular organization of the cytoplasm. *Curr. Opin. Struct. Biol.* **12**, 679–684 (2002).
20. Hagen, W. J. H., Wan, W. & Briggs, J. A. G. Implementation of a cryo-electron tomography tilt-scheme optimized for high resolution subtomogram averaging. *J. Struct. Biol.* **197**, 191–198 (2017).
21. Grünewald, K. *et al.* Three-dimensional structure of herpes simplex virus from cryo-electron tomography. *Science* **302**, 1396–1398 (2003).
22. Förster, F., Medalia, O., Zauberman, N., Baumeister, W. & Fass, D. Retrovirus envelope protein complex structure in situ studied by cryo-electron tomography. *Proc. Natl. Acad. Sci. U. S. A.* **102**, 4729–4734 (2005).
23. Murphy, G. E., Leadbetter, J. R. & Jensen, G. J. In situ structure of the complete *Treponema primitia* flagellar motor. *Nature* **442**, 1062–1064 (2006).
24. Ghosal, D., Chang, Y.-W., Jeong, K. C., Vogel, J. P. & Jensen, G. J. In situ structure of the Legionella Dot/Icm type IV secretion system by electron cryotomography. *EMBO Rep.* **18**, 726–732 (2017).
25. Chang, Y.-W., Shaffer, C. L., Rettberg, L. A., Ghosal, D. & Jensen, G. J. structures of the type IV secretion system. (2017). doi:10.1101/195685
26. Chang, Y., Rettberg, L. A., Ortega, D. R. & Jensen, G. J. *In vivo* structures of an intact type VI secretion system revealed by electron cryotomography. *EMBO Rep.* **18**, 1090–1099 (2017).

27. Chang, Y.-W. *et al.* Architecture of the *Vibrio cholerae* toxin-coregulated pilus machine revealed by electron cryotomography. *Nat. Microbiol.* **2**, 16269 (2017).
28. Chang, Y.-W. *et al.* Correlated cryogenic photoactivated localization microscopy and cryo-electron tomography. *Nat. Methods* **11**, 737–739 (2014).
29. Kukulski, W. *et al.* Correlated fluorescence and 3D electron microscopy with high sensitivity and spatial precision. *J. Cell Biol.* **192**, 111–119 (2011).
30. Danev, R., Buijsse, B., Khoshouei, M., Plitzko, J. M. & Baumeister, W. Volta potential phase plate for in-focus phase contrast transmission electron microscopy. *Proc. Natl. Acad. Sci. U. S. A.* **111**, 15635–15640 (2014).
31. Campbell, M. G. *et al.* Movies of ice-embedded particles enhance resolution in electron cryo-microscopy. *Struct. Lond. Engl. 1993* **20**, 1823–1828 (2012).
32. Kühlbrandt, W. Biochemistry. The resolution revolution. *Science* **343**, 1443–1444 (2014).
33. McMullan, G., Faruqi, A. R., Clare, D. & Henderson, R. Comparison of optimal performance at 300keV of three direct electron detectors for use in low dose electron microscopy. *Ultramicroscopy* **147**, 156–163 (2014).
34. Jeong, K. C., Ghosal, D., Chang, Y.-W., Jensen, G. J. & Vogel, J. P. Polar delivery of *Legionella* type IV secretion system substrates is essential for virulence. *Proc. Natl. Acad. Sci. U. S. A.* **114**, 8077–8082 (2017).
35. Chen, S. *et al.* Structural diversity of bacterial flagellar motors. *EMBO J.* **30**, 2972–2981 (2011).
36. Kudryashev, M. *et al.* In situ structural analysis of the *Yersinia enterocolitica* injectisome. *eLife* **2**, e00792 (2013).
37. Nans, A., Kudryashev, M., Saibil, H. R. & Hayward, R. D. Structure of a bacterial type III secretion system in contact with a host membrane in situ. *Nat. Commun.* **6**, 10114 (2015).
38. Böck, D. *et al.* In situ architecture, function, and evolution of a contractile injection system. *Science* **357**, 713–717 (2017).
39. Yeo, H. J., Savvides, S. N., Herr, A. B., Lanka, E. & Waksman, G. Crystal structure of the hexameric traffic ATPase of the *Helicobacter pylori* type IV secretion system. *Mol. Cell* **6**, 1461–1472 (2000).
40. Chandran, V. *et al.* Structure of the outer membrane complex of a type IV secretion system. *Nature* **462**, 1011–1015 (2009).

41. Gendrin, C. *et al.* Structural basis of cytotoxicity mediated by the type III secretion toxin ExoU from *Pseudomonas aeruginosa*. *PLoS Pathog.* **8**, e1002637 (2012).
42. Zoued, A. *et al.* Priming and polymerization of a bacterial contractile tail structure. *Nature* **531**, 59–63 (2016).
43. Fullner, K. J., Lara, J. C. & Nester, E. W. Pilus assembly by *Agrobacterium* T-DNA transfer genes. *Science* **273**, 1107–1109 (1996).
44. Iancu, C. V. *et al.* Electron cryotomography sample preparation using the Vitrobot. *Nat. Protoc.* **1**, 2813–2819 (2006).
45. Tivol, W. F., Briegel, A. & Jensen, G. J. An improved cryogen for plunge freezing. *Microsc. Microanal. Off. J. Microsc. Soc. Am. Microbeam Anal. Soc. Microsc. Soc. Can.* **14**, 375–379 (2008).
46. Suloway, C. *et al.* Automated molecular microscopy: the new Legimon system. *J. Struct. Biol.* **151**, 41–60 (2005).
47. Mastronarde, D. N. Automated electron microscope tomography using robust prediction of specimen movements. *J. Struct. Biol.* **152**, 36–51 (2005).
48. Zheng, S. Q. *et al.* UCSF tomography: an integrated software suite for real-time electron microscopic tomographic data collection, alignment, and reconstruction. *J. Struct. Biol.* **157**, 138–147 (2007).
49. Zheng, S. Q. *et al.* MotionCor2: anisotropic correction of beam-induced motion for improved cryo-electron microscopy. *Nat. Methods* **14**, 331–332 (2017).
50. Kremer, J. R., Mastronarde, D. N. & McIntosh, J. R. Computer visualization of three-dimensional image data using IMOD. *J. Struct. Biol.* **116**, 71–76 (1996).
51. Mastronarde, D. N. Correction for non-perpendicularity of beam and tilt axis in tomographic reconstructions with the IMOD package. *J. Microsc.* **230**, 212–217 (2008).
52. Agulleiro, J.-I. & Fernandez, J.-J. Tomo3D 2.0--exploitation of advanced vector extensions (AVX) for 3D reconstruction. *J. Struct. Biol.* **189**, 147–152 (2015).
53. Nicastro, D. *et al.* The molecular architecture of axonemes revealed by cryoelectron tomography. *Science* **313**, 944–948 (2006).
54. Hrabe, T. *et al.* PyTom: a python-based toolbox for localization of macromolecules in cryo-electron tomograms and subtomogram analysis. *J. Struct. Biol.* **178**, 177–188 (2012).

55. Bharat, T. A. M. & Scheres, S. H. W. Resolving macromolecular structures from electron cryotomography data using subtomogram averaging in RELION. *Nat. Protoc.* **11**, 2054–2065 (2016).
56. Castaño-Díez, D., Kudryashev, M., Arheit, M. & Stahlberg, H. Dynamo: a flexible, user-friendly development tool for subtomogram averaging of cryo-EM data in high-performance computing environments. *J. Struct. Biol.* **178**, 139–151 (2012).
57. Pettersen, E. F. *et al.* UCSF Chimera--a visualization system for exploratory research and analysis. *J. Comput. Chem.* **25**, 1605–1612 (2004).
58. Kucukelbir, A., Sigworth, F. J. & Tagare, H. D. Quantifying the local resolution of cryo-EM density maps. *Nat. Methods* **11**, 63–65 (2014).

Figure: 1

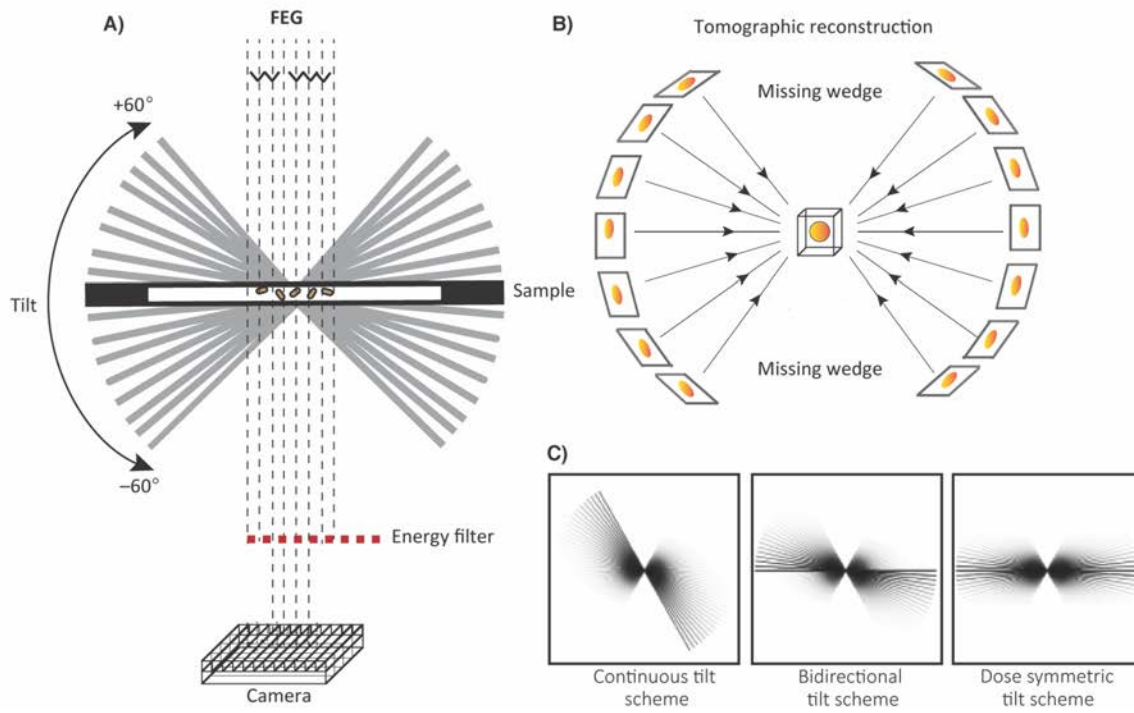


Figure: 2

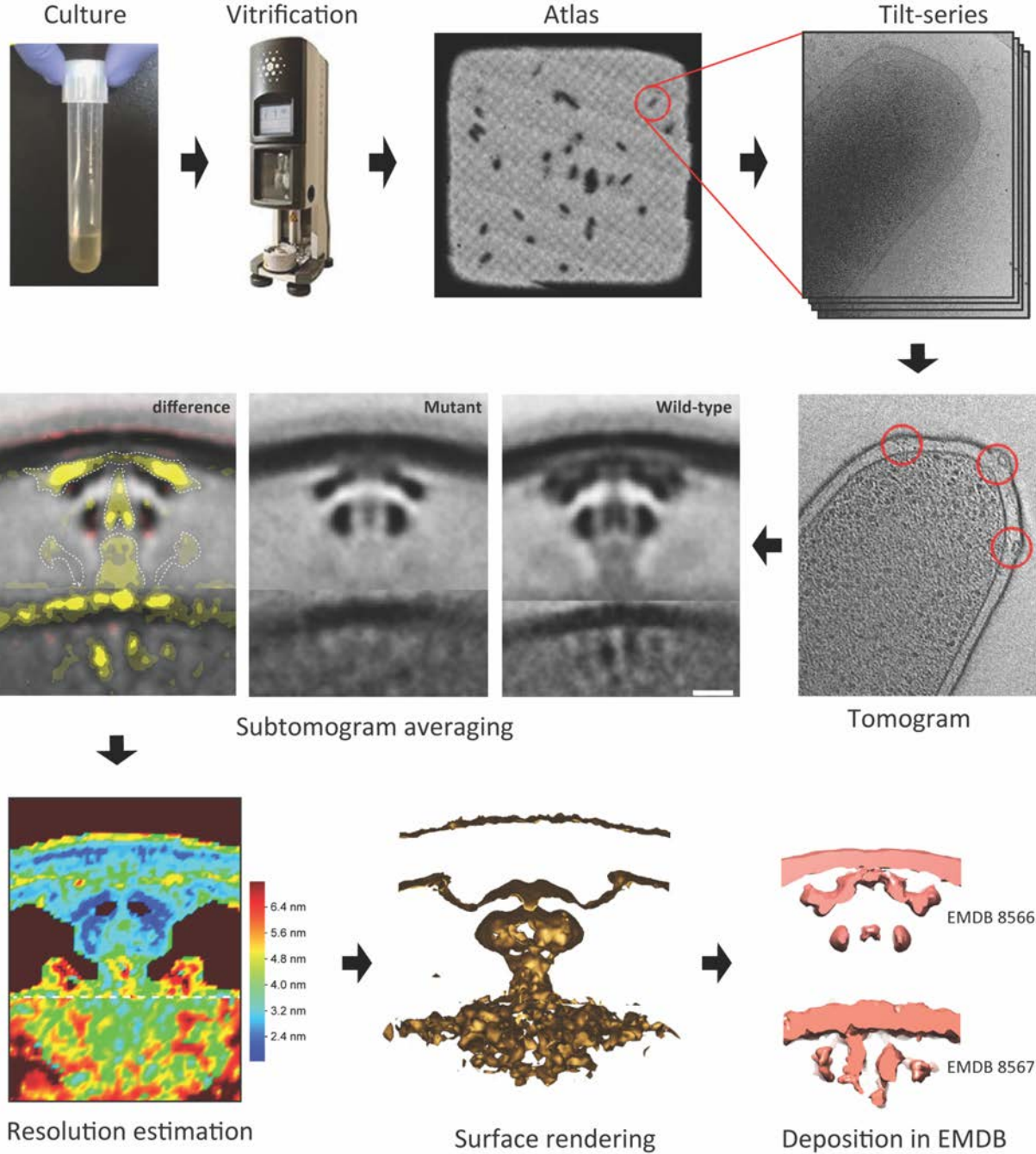


Figure: 3

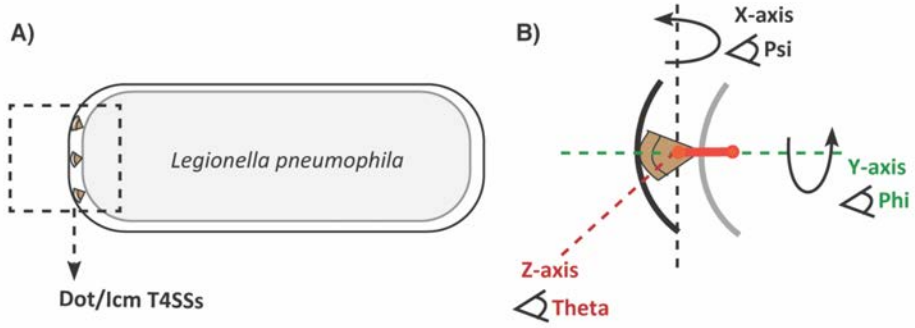


Table-1

UCSF TOMO. mode	Magnification	Defocus (um)	Slit width (eV)	Exposure time (s)	Binning	Spot size	Pixel size (Å)	Camera mode
Atlas	3000x	-40	40	0.5	4	11	37	Counted
Search	9300x	-20	20	0.5	2	11	12	Counted
Track	9300x	0	20	0.5	2	11	12	Counted
Focus	27,500x	0	20	0.5	2	11	3.9	Counted
Collect	27,500x	-6	20	As determined	1	11	3.9	Counted

Table-2

Run	Angular search range						Search Distance	High Frequency Filter		Ref. Threshold
	Phi		Theta		Psi			Cutoff	Sigma	
	Max	Min	Max	Min	Max	Min				
1	180	20	0	0	0	0	5	0.25	0.05	2/3 of all particles
2	30	10	30	10	30	10	3	0.25	0.05	2/3 of all particles
3	15	5	15	5	15	5	3	0.25	0.05	2/3 of all particles
4	7.5	2.5	7.5	2.5	7.5	2.5	2	0.25	0.05	2/3 of all particles
5	3.75	1.25	3.75	1.25	3.75	1.25	2	0.25	0.05	2/3 of all particles
6	1.875	0.625	1.875	0.635	1.875	0.635	2	0.25	0.05	2/3 of all particles